3-D Short-Range Imaging With Irregular MIMO Arrays Using NUFFT-Based Range Migration Algorithm

I. Objective

Propose an efficient 3D imaging algorithm for arbitrary 2D planar MIMO arrays to overcome limitations in speed and array structure constraints.

II. Introduction

A. Applications of Microwave Antenna Arrays
   1. Concealed weapon detection
   2. Ground-penetrating radar (GPR)
   3. Through-wall imaging

B. Methods to Achieve High Cross-Range Resolution
   1. Phased Array
      a. Controls beam direction via phase adjustment
      b. Higher resolution with more antennas, but at higher cost
   2. Synthetic Aperture Radar (SAR)
      a. Simulates a larger antenna array by physically moving a smaller antenna array
   3. MIMO Array

< Explanation >

Although both MIMO and SAR can effectively reduce the number of physical antennas required, the total number of antennas is still limited, leading to a restricted field of view. As a result, the imaging range is confined to short distances.

C. Evolution of Methods in 3D Imaging
   1. True 3D imaging requires a 2D antenna array
      a. Frequency and time data in received signals determine object distance (third dimension)
   2. SAR only Strategy
      a. A linear array is moved along the second direction to simulate a 2D antenna array.

b. 3 Scanning Configurations
    1. Linear scanning: perpendicular to the array, used in GPR
    2. Cylindrical scanning: array rotates around a parallel axis, used in airport body scanners
    3. Radial scanning (Rad-SAR): array rotates in-plane around its center, suitable for tunnel inspection
c. Even though SAR techniques can synthesize a larger aperture along the scanning direction, the resolution along the original linear array axis remains unchanged unless the physical length of the linear array is increased. Therefore, a large linear array is still required, which is not cost-effective.

3. SAR + MIMO Strategy
    a. Replace linear array in SAR with a 1D MIMO array, and move the 1D MIMO array to synthesize a 2D MIMO array
    b. Imaging Algorithm Options
        1. Traditional Methods
            a. For example: Filtered Backprojection, Kirchhoff Migration
            b. Applicable to arbitrary antenna configurations with high accuracy, but extremely computationally intensive and slow
            c. Often rely on inversion-based algorithms, which reconstruct the object distribution or scene by back-calculating from observed data. These methods do not depend on FFT operations or require regular antenna configurations, making them suitable for arbitrary array geometries. However, they typically involve solving large-scale optimization problems—such as matrix inversion or gradient-based minimization—which are computationally intensive. Although iterative solvers have been proposed to address these problems, they may require thousands of iterations to converge, posing significant challenges for real-time imaging in large-scale arrays or high-resolution scenarios.
        2. Hybrid Migration
            a. For example: Fourier-summation-based migration
            b. Replace integration with FFT to accelerate imaging

c. However, requires 1D MIMO array to be uniformly spaced

4. 2D MIMO Strategy
   a. Data Acquisition Problem in SAR+MIMO
      1. Since SAR+MIMO relies on mechanically moving or rotating a linear MIMO array, the data acquisition process is typically time-consuming. This limits its applicability in scenarios that require rapid response or real-time imaging, as the acquisition speed is insufficient.
      2. To address this limitation, it is more effective to replace the 1D MIMO array combined with SAR with a 2D MIMO array
         a. By employing orthogonal waveforms or time-division multiplexing across the transmit antennas, the system can simultaneously acquire data from all MIMO channels within a single measurement, making it suitable for real-time applications.
         b. The spatial diversity of a 2D MIMO array enables the synthesis of a large effective aperture using fewer physical antennas. Specifically, a 2D MIMO array provides $N_t \times N_r$ channels with only $N_t + N_r$ antennas, significantly reducing system cost without compromising imaging quality.
5. New Strategy Proposed in This Paper: NUFFT-based MIMO-RMA
   a. Efficient 3D Imaging Algorithm for 2D MIMO Arrays
   b. Frequency-Domain Acceleration Using RMA

      The Range Migration Algorithm (RMA) transforms conventional spatial-domain integration into frequency-domain multiplication via FFT (Fast Fourier Transform), significantly improving processing speed over direct inversion-based methods.
   c. Transverse Spectrum Deconvolution for 5D to 3D Mapping

      To further enhance imaging efficiency, a transverse spectrum deconvolution technique is introduced. This module performs the critical dimensionality reduction from the original 5D MIMO frequency domain representation — defined over transmit and receive antenna positions $(\mathrm{f}, \mathrm{k}_{\mathrm{x_t}}, k_{z_t}, k_{x_r}, k_{z_r})$ and frequency — to a 3D spatial image cube (x, y, z).
   d. Support for Arbitrary 2D MIMO Arrays via NUFFT

Since RMA and FFT inherently require uniform antenna sampling, the paper incorporates the Non-Uniform Fast Fourier Transform (NUFFT) to accommodate arbitrary (non-uniformly spaced) 2D MIMO arrays. The NUFFT maps the irregular spatial domain samples onto a uniform grid in the frequency-wavenumber (f–k) domain, enabling FFT-based acceleration while preserving accuracy.

e. Energy Compensation via Voronoi-Based Weighting

To address uneven spatial sampling and the resulting energy distortion in the spectrum, Voronoi decomposition is used to compute the effective coverage area of each antenna. These areas are then employed to weight the spectral contribution of each antenna during NUFFT, achieving accurate compensation for spatial non-uniformity.

f. Replacing Interpolation with 1D NUFFT for Curvature Correction

Traditional curvature correction involves interpolation, which is both computationally expensive and potentially inaccurate. This work proposes the use of 1D NUFFT to directly approximate frequency-domain shifts from non-uniform samples. This approach not only eliminates the need for time-consuming interpolation but also improves reconstruction fidelity.

III. Derivation

A. Modeling Assumptions

1. The Born approximation is assumed to be valid, implying that the incident wave is not significantly altered by the target.
2. A scalar wave model is adopted, where polarization effects of the electromagnetic (EM) wave are neglected; only amplitude and phase are considered.
3. All antennas are assumed to be isotropic radiators.
4. A 2D MIMO antenna array is placed on the x–z plane, while the imaging target is located along the y-axis (i.e., in front of the array).
5. The targets are assumed to lie within the near-field region of the MIMO array, hence spherical wavefront propagation must be taken into account for accurate modeling, particularly for high-resolution imaging.

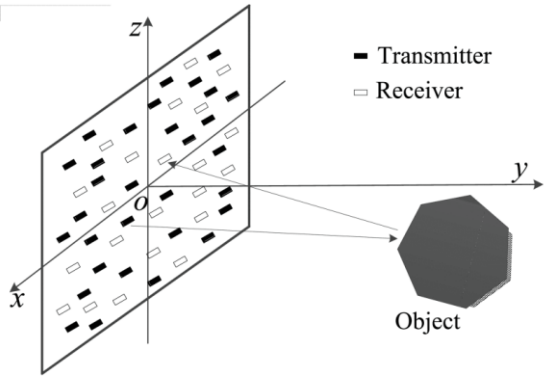

B. For a given pair of transmit and receive antennas located at $(\mathrm{x_t}, z_t, 0)$ and $(x_r, z_r, 0)$, respectively, the received scattered signal can be expressed as:

$$\mathrm{s(t, x_t, z_t}, x_r, z_r) = \iiint_V \frac{f(x,y,z)}{16\pi^2 R_t R_r} \cdot p\left(t - \frac{R_t}{c} - \frac{R_r}{c}\right) dxdydz \quad (1)$$

$\mathrm{(x, y, z)}$: location of the object

$\mathrm{f(x, y, z)}$: scattering coefficient of the object

V: volume occupied by the illuminated targets

c: speed of the electromagnetic (EM) wave

p(t): radiated signal

$\mathrm{R_t/R_r}$: distances from the transmitter/receiver to the object

$$\begin{cases} R_t = \sqrt{(x - x_t)^2 + y^2 + (z - z_t)^2} \\ R_r = \sqrt{(x - x_r)^2 + y^2 + (z - z_r)^2} \end{cases}$$

1. The total time delay is given by $\frac{R_t}{c} - \frac{R_r}{c}$, which shifts the transmitted waveform

   $\mathrm{p(t)} \rightarrow p\left(t - \frac{R_t}{c} - \frac{R_r}{c}\right)$

2. This delayed waveform is modulated by the object's scattering coefficient $\mathrm{f(x, y, z)}$, and attenuated by the spherical spreading factor $\frac{1}{16\pi^2 R_t R_r}$, yielding the contribution of one scattering point.
3. Integrating over the entire illuminated volume VVV results in the total received signal.

C. Taking the Fourier Transform of Equation (1) with respect to time t, we obtain:

$$\mathrm{s(f, x_t, z_t}, x_r, z_r) = \iiint_V \frac{f(x,y,z)}{16\pi^2 R_t R_r} \cdot P(f) e^{-jk(R_t + R_r)} dxdydz \quad (2)$$

$\mathrm{k} = \frac{2\pi \mathrm{f}}{\mathrm{c}}$: $wavenumber\ related\ to\ the\ frequency\ f$

$\mathrm{P(f)}$: $\mathbb{F}\{\mathrm{p(t)}\}$

D. Spherical Wave Expansion Using Weyl Identity

$$\mathrm{s(f, x_t, z_t, x_r, z_r)} = \iiint_V f(x,y,z)\cdot P(f)dxdydz$$

$$\cdot \iint -\frac{\mathrm{je}^{-\mathrm{j(k_{x_t}x+k_{y_t}y+k_{z_t}z)}}}{8\pi^2 k_{y_t}}\, e^{j(k_{x_t}x_t+k_{z_t}z_t)}dk_{x_t}dk_{z_t} \quad \text{(Spherical wave expansion from the Tx)}$$

$$\cdot \iint -\frac{\mathrm{je}^{-\mathrm{j(k_{x_r}x+k_{y_r}y+k_{z_r}z)}}}{8\pi^2 k_{y_r}}\, e^{j(k_{x_r}x_r+k_{z_r}z_r)}dk_{x_r}dk_{z_r} \quad \text{(Spherical wave expansion from the Rx)} \quad (3)$$

$\mathrm{k_{x_t}}, k_{z_t}, k_{x_r}, k_{z_r}$: Fourier counterparts of $\mathrm{x_t}, z_t, x_r, z_r$ in the wavenumber domain

$$\begin{cases} \mathrm{k_{y_t}} = \sqrt{k^2 - \mathrm{k_{x_t}^2} - k_{z_t}^2} \\ \mathrm{k_{y_r}} = \sqrt{k^2 - \mathrm{k_{x_r}^2} - k_{z_r}^2} \end{cases}$$

E. Replace the variables $\mathrm{x_t}, \mathrm{z_t}, x_r, z_r$ in equation (3) with $\mathrm{k_{x_t}}, k_{z_t}, k_{x_r}, k_{z_r}$

$$(3) \Rightarrow \mathrm{S(f, k_{x_t}}, k_{z_t}, k_{x_r}, k_{z_r}) = -\frac{P(f)}{4k_{y_t}k_{y_r}} \iiint_V f(x,y,z)e^{-j(k_x x+k_y y+k_z z)}dxdydz \quad (4)$$

$$\begin{cases} k_x = k_{x_t} + k_{x_r} \\ k_y = k_{y_t} + k_{y_r} \\ k_z = k_{z_t} + k_{z_r} \end{cases}$$

$-\frac{P(f)}{4k_{y_t}k_{y_r}}$: the constant term obtained from the spherical wave expansion

F. $(4) \Rightarrow \mathrm{S(f, k_{x_t}}, k_{z_t}, k_{x_r}, k_{z_r}) \underset{F.T}{\overset{F.T^{-1}}{\rightleftarrows}} f(x,y,z)$

$$\Rightarrow \begin{cases} F.T.^{-1} \longrightarrow \mathrm{S(f, k_{x_t}}, k_{z_t}, k_{x_r}, k_{z_r}) = -\frac{P(f)}{4k_{y_t}k_{y_r}} \iiint_V f(x,y,z)e^{-j(k_x x+k_y y+k_z z)}dxdydz \\ F.T. \longrightarrow f(x,y,z) = \frac{1}{2\pi^3} \iiint \frac{k_{y_t}k_{y_r}}{P(f)} \mathrm{S(f, k_{x_t}}, k_{z_t}, k_{x_r}, k_{z_r}) \cdot e^{j(k_x x+k_y y+k_z z)}dk_x dk_y dk_z \end{cases}$$

G. Conclusion

we can reconstruct the object's image using the inverse Fourier transform.

IV. Efficient implementation of the inverse Fourier transform

A. Apply 1D Fourier Transform with respect to time

$$\mathrm{s(t, x_t, z_t, x_r, z_r)} \rightarrow \mathrm{s(f, x_t, z_t, x_r, z_r)}$$

B. Apply two 2D spatial transforms over the transmit and receive antenna planes

$$\mathrm{s(f, x_t, z_t, x_r, z_r)} \rightarrow \mathrm{S(f, k_{x_t}}, k_{z_t}, k_{x_r}, k_{z_r})$$

This can be expressed as

$$S(f, k_{x_t}, k_{z_t}, k_{x_r}, k_{z_r}) = \iint_{(x_t,z_t)} \iint_{(x_r,z_r)} s(f, x_t, z_t, x_r, z_r) e^{-j(k_{x_t}x_t + k_{z_t}z_t)} e^{-j(k_{x_r}x_r + k_{z_r}z_r)} dx_t dz_t dx_r dz_r$$

1. However, since the antennas are not uniformly distributed in space, a 2D FFT cannot be directly applied and must be replaced by a Riemann sum.

$$S(f, k_{x_t}, k_{z_t}, k_{x_r}, k_{z_r}) = \sum_{m=0}^{N_t-1} \sum_{n=0}^{N_r-1} s(f, x_{t_m}, z_{t_m}, x_{r_n}, z_{r_n})\, e^{-j(k_{x_t}x_{t_m} + k_{z_t}z_{t_m})} e^{-j(k_{x_r}x_{r_n} + k_{z_r}z_{r_n})} \Delta S_{t_m} \Delta S_{r_n} \quad (5)$$

(x_{t_m}, z_{t_m}) *and* (x_{r_n}, z_{r_n}): locations of the m-th Tx antenna and n-th Rx antenna

$\Delta S_{t_m}, \Delta S_{r_n}$: area weights computed using Voronoi decomposition, compensating for non-uniform spatial sampling.

2. To avoid the high computational cost of direct summation, we apply Non-Uniform FFT (NUFFT) to accelerate the computation

$$S(f, k_{x_t}, k_{z_t}, k_{x_r}, k_{z_r}) = \sum_{m=0}^{N_t-1} e^{-j(k_{x_t}x_{t_m} + k_{z_t}z_{t_m})} \Delta S_{t_m} \cdot \left[\sum_{n=0}^{N_r-1} s(f, x_{t_m}, z_{t_m}, x_{r_n}, z_{r_n}) \Delta S_{r_n} \cdot e^{-j(k_{x_r}x_{r_n} + k_{z_r}z_{r_n})} \right] \quad (6)$$

(5) is a 4D nonuniform discrete FT(NDFT)

Rewrite (5) as two 2D NDFTs, separated into receiver and transmitter stages, to reduce computational complexity.

Each NDFT is then accelerated using NUFFT, resulting in two 2D NUFFT operations.

C. 5D to 3D mapping

1. After obtaining $S(f, k_{x_t}, k_{z_t}, k_{x_r}, k_{z_r})$ on a 5D uniform grid, we map it onto a 3D uniform grid (k_x, k_y, k_z), enabling reconstruction in the spatial domain (x, y, z)

2. As mentioned above, $\begin{cases} k_x = k_{x_t} + k_{x_r} \\ k_y = k_{y_t} + k_{y_r} \\ k_z = k_{z_t} + k_{z_r} \end{cases}$

Since $k_{x_t}, k_{z_t}, k_{x_r}, k_{z_r}$ are uniformly distributed, k_x and k_z are also uniformly distributed.

However, $\begin{cases} \mathrm{k_{y_t}} = \sqrt{k^2 - \mathrm{k_{x_t}^2} - k_{z_t}^2} \\ \mathrm{k_{y_r}} = \sqrt{k^2 - \mathrm{k_{x_r}^2} - k_{z_r}^2} \end{cases}$

These two components are derived from $\mathrm{k_{x_t}}, k_{z_t}, k_{x_r}, k_{z_r}$, and thus are not uniformly distributed. Consequently, k_y is also non-uniformly distributed.

3. We need to apply Stolt interpolation to transform k_y into a uniformly distributed variable. However, this interpolation process involves a high computational cost and may introduce interpolation errors.
4. Therefore, we replace the interpolation method on k_y with 1D NUFFT, which also allows us to omit the subsequent IFFT step. This substitution significantly improves both computational efficiency and reconstruction accuracy.

D. The 3D IFFT completes the image reconstruction from $(k_x, k_y, k_z) \rightarrow (\mathrm{x}, \mathrm{y}, \mathrm{z})$. If k_y is processed using NUFFT, then only a 2D IFFT is required.

E. The following is the flowchart of the algorithm

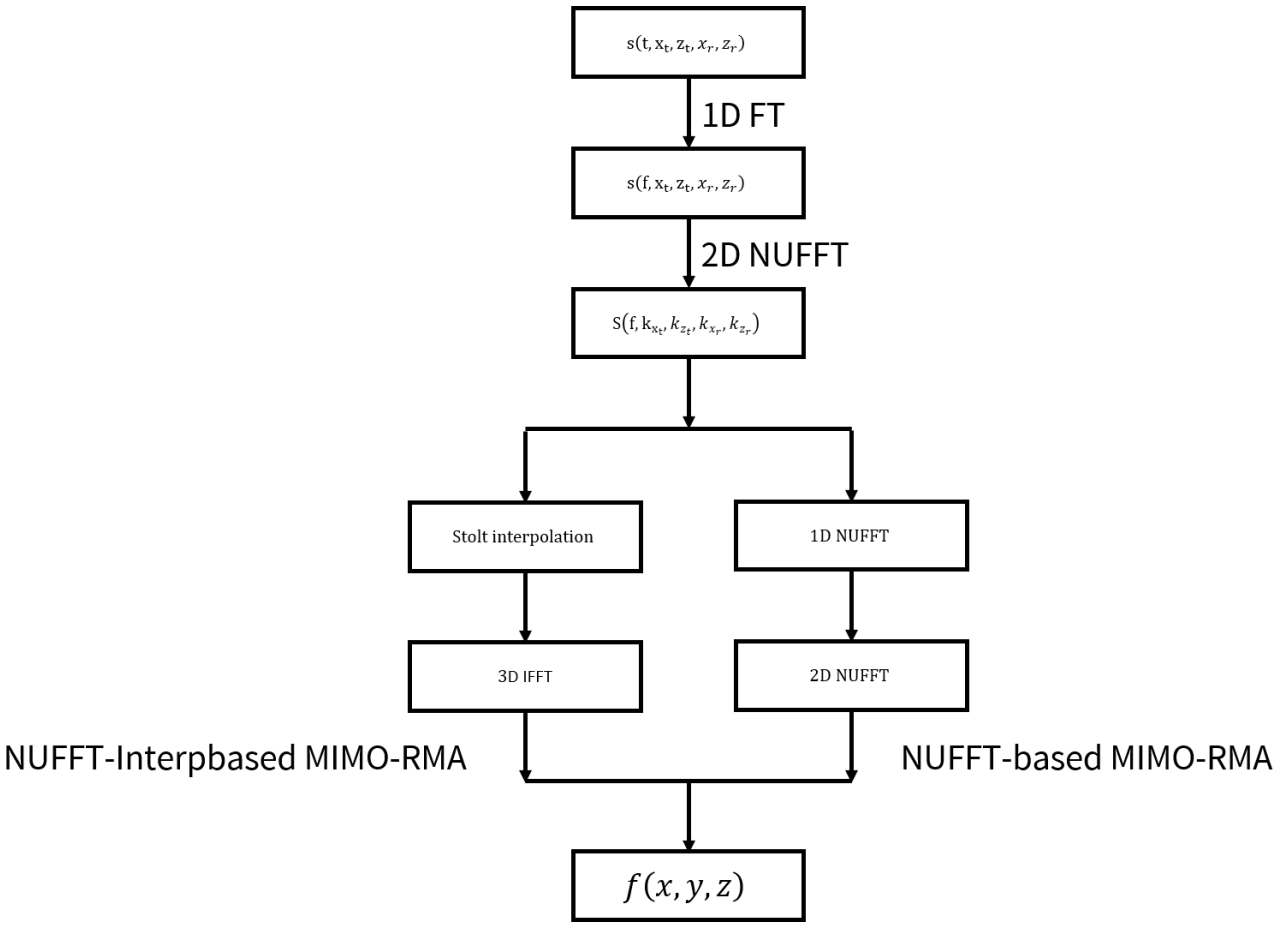

V. Implementation Issues

A. $s(t, x_t, z_t, x_r, z_r) \rightarrow s(f, x_t, z_t, x_r, z_r)$

For different Radar system types:

1. Pulse-based systems: Since the signal is in the time domain, an FFT is required.
2. Step-frequency systems: The signal is already in the frequency domain, so this step can be skipped.

B. $s(f, x_t, z_t, x_r, z_r) \rightarrow S(f, k_{x_t}, k_{z_t}, k_{x_r}, k_{z_r})$

To avoid aliasing, the sampling intervals in the wavenumber domain must satisfy the Nyquist criterion.

Assuming the field of view (FOV) of the 2D antenna array is a×b, the required sampling intervals are:

$$\begin{cases} \Delta k_{x_t} \le \frac{2\pi}{a}, \Delta k_{z_t} \le \frac{2\pi}{b} \\ \Delta k_{x_r} \le \frac{2\pi}{a}, \Delta k_{z_r} \le \frac{2\pi}{b} \end{cases}$$

$\Delta k_{x_t}, \Delta k_{x_r}$: sampling intervals along the k_x and k_z directions

Let $\Delta k_{x_t} = \Delta k_{x_r}, \Delta k_{z_t} = \Delta k_{z_r}$ to simplify the subsequent 5D to 3D mapping process.

Given the sampling interval Δk, the number of samples along each dimension $(k_{x_t}, k_{z_t}, k_{x_r}, k_{z_r})$ is decided.

$$\because \begin{cases} k_{max} = \frac{2\pi}{\lambda} = \frac{2\pi f_{max}}{c} \\ N = \frac{k_{max}}{\Delta k} \end{cases} \Rightarrow N = \frac{2\pi f_{max}}{c \cdot \Delta k} \qquad \therefore \begin{cases} N_{k_x}^t = \frac{2\pi f_{max}}{c \cdot \Delta k_{x_t}}, N_{k_z}^t = \frac{2\pi f_{max}}{c \cdot \Delta k_{z_t}} \\ N_{k_x}^r = \frac{2\pi f_{max}}{c \cdot \Delta k_{x_r}}, N_{k_z}^r = \frac{2\pi f_{max}}{c \cdot \Delta k_{z_r}} \end{cases}$$

If there are M frequency sampling points, the total data size is:

$$N_{k_x}^t \times N_{k_z}^t \times N_{k_x}^r \times N_{k_z}^r \times M$$

1. Region of Support (ROS) Optimization
   a. To reduce data volume and computation, only frequency components within the region of support (ROS) are processed (i.e., $f < f_{max}$). Frequencies outside the ROS are zero-padded.
   b. The reduced number of samples for each frequency:

$$\begin{cases} N_{k_x}^t = \dfrac{2\pi f}{c \cdot \Delta k_{x_t}}, N_{k_z}^t = \dfrac{2\pi f}{c \cdot \Delta k_{z_t}} \\ N_{k_x}^r = \dfrac{2\pi f}{c \cdot \Delta k_{x_r}}, N_{k_z}^r = \dfrac{2\pi f}{c \cdot \Delta k_{z_r}} \end{cases}, \quad for\ \mathrm{f} < \mathrm{f_{max}}$$

2. parallel computation
   Each frequency slice is processed independently, allowing for parallel computation across frequencies to improve speed.

C. $f(x,y,z) = \frac{1}{2\pi^3} \iiint \frac{k_{y_t} k_{y_r}}{P(f)} \mathrm{S}(\mathrm{f}, \mathrm{k_{x_t}}, k_{z_t}, k_{x_r}, k_{z_r}) \cdot e^{j(k_x x + k_y y + k_z z)} dk_x dk_y dk_z$

1. Before reconstruction, the spectral data is multiplied by the weighting factor: $\frac{k_{y_t} k_{y_r}}{2\pi^3 P(f)}$. This step serves both as a compensation for earlier Voronoi weighting and as a high-pass filter in the f-k domain.
   If the noise level is high, a better filter may be used to reduce errors. However, such filters would need to be designed for every combination of $(\mathrm{k_{x_t}}, k_{z_t}, k_{x_r}, k_{z_r})$, drastically increasing computational complexity.

VI. Simulation Results of the Proposed Method

		Array I		Array II	
		9-12GHz	5-15GHz	9-12GHz	5-15GHz
NUFFT-based RMA	α	0.3641	0.2891	0.6369	0.5630
	Time[s]	36	53	36	53
NUFFT-Interp-based RMA	α	0.3664	0.2943	0.6990	0.5772
	Time[s]	104	123	103	122
Kirchhoff migration	α	0.2539	0.1853	0.2782	0.2343
	Time[s]	518	520	172	173

A. Kirchhoff migration is used as the baseline for comparison, representing traditional approaches to image reconstruction.

B. $\alpha = \frac{P_o}{P_i}$:

power spreading ratio defined as the power spreading outside the object normalized to the power within the object volume

C. Computation Time
NUFFT-based MIMO-RMA > NUFFT-Interp-based MIMO-RMA > Kirchhoff migration

D. Noise Level
NUFFT-Interp-based MIMO-RMA > NUFFT-based MIMO-RMA > Kirchhoff migration

E. Effect of Increased Bandwidth

1. As the bandwidth increases, the pulse width of the time-domain signal decreases, resulting in sharper imaging and reduced noise.
2. Signals received from different antenna pairs become more distinguishable, improving imaging resolution.
3. All three methods show significant improvements in image quality under increased bandwidth conditions.

F. Computation Time vs. Bandwidth
1. When the bandwidth increases, both NUFFT-based and NUFFT-Interp-based MIMO-RMA show a significant rise in computational time.
2. In contrast, the computational time of Kirchhoff migration remains nearly constant.
   This is because Kirchhoff migration operates in the time–spatial domain, and is not directly affected by the number of frequency samples.

G. Performance Under Sparse Array Conditions
1. Under sparse array configurations, all three methods exhibit increased noise levels. However, Kirchhoff migration still maintains relatively good image quality.
2. Additionally, due to the reduced number of spatial sampling points, the overall data volume decreases, leading to a substantial reduction in computation time for Kirchhoff migration.
3. In contrast, both NUFFT-based and NUFFT-Interp-based MIMO-RMA maintain nearly constant computation time, as their operations are conducted over a fixed-size f–k domain grid.
4. Furthermore, the increased antenna spacing in sparse arrays leads to insufficient spatial sampling, which causes aliasing artifacts during FFT-based processing and significantly degrades the imaging quality.

VII. Conclusion

A. For dense MIMO arrays, the NUFFT-based MIMO-RMA is the preferred method due to its high imaging efficiency and resolution.
B. For ultrasparse MIMO arrays, a modified Kirchhoff migration method is more suitable, as it provides better robustness to sparse sampling and reduced computational load.

VIII. My MATLAB Simulation

A. Implemented the NUFFT-based MIMO-RMA algorithm in MATLAB.

B. Utilized an appropriate dataset for algorithm testing and verification.
   Dataset source: https://ieee-dataport.org/open-access/em-data-acquired-irregular-planar-mimo-arrays

C. Simulation result